CHAPTER VIII

SOME NEW OBSERVATIONS ON ELECTROHYDRODYNAMIC INSTABILITIES IN NEMATIC LIQUID CRYSTALS

Introduction

As mentioned in Chapter I, the effect of electric field effects on the alignment of liquid crystals is somewhat complicated. As early as 1931, Kast had observed that the alignment of the molecules in a nematic liquid crystal by a low frequency electric field is quite different compared to that by a high frequency field. Zwetkoff and Mikhailov (1938) suggested that the alignment at low frequency could be due to the anisotropic conductivity. Carr (1963) proved that the electric conduction plays an important role in the molecular alignment.

When dielectric and conductivity anisotropies are of opposite sign an electrohydrodynamic instability sets in beyond a threshold voltage in a nematic liquid crystal subjected to an electric field in an appropriate geometry. Such an observation was made long back in 1933 by Freedericksz and Zolina.

More recently Williams (1963) observed that when a thin film of nematic liquid crystal having negative

dielectric anisotropy, contained between two conducting glass plates (figure 8.1) is subjected to a D.C. or low frequency A.C. field, striations are seen beyond a voltage threshold. These striations are now referred to as 'Williams domains'. The geometry is known as the sandwich geometry. In a homogeneously aligned sample, the striations are normal to the undistorted $\vec{n}$. The domains are seen in the absence of polarisers. If incident light is polarized normal to the undistorted $\vec{n}$, the domains are invisible (Helfrich 1969). This suggested that tho modifications of $\vec{n}$ takes place in the field direction. As the voltage is increased much above the threshold value, turbulence sets in. The liquid crystal is then said to go over to the 'dynamic scattering mode' (Heilmeier et al. 1968).

When an electric field is applied to a nematic liquid crystal of negative dielectric anisotropy, the dielectrically stable configuration is when $\vec{n}$ is normal to $\vec{E}$. However, the space charges induced by the field can give rise to anomalous alignment. Initiated by this conclusion of Carr (1963) that the electrical conductivity is an important factor in the anomalous alignment, Helfrich (1969) gave a model for the D.C. field case to explain such an alignment.

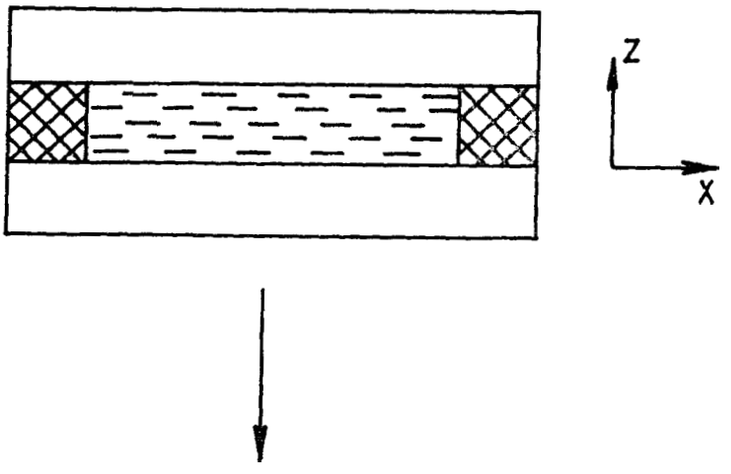

Figure 8.1

The sandwich geometry for observing William's domains. The electric field is applied along the Z direction. The arrow shows the direction of observation(parallel to Z axis).

A nematic liquid crystal is basically a good electrical insulator. However, there always exists some ionic impurity in the sample. Usually the conductivity anisotropy is positive since it is easier for the ions to move along $\vec{n}$ rather than normal to it.

In the 'sandwich' geometry with parallel to the glass plates, due to thermal fluctuations $\vec{n}(x,t)$ is not strictly normal to $\vec{E}$ but fluctuates about a mean value. We shall consider a bend fluctuation as shown in figure 8.2. As a result of these fluctuations and positive conductivity anisotropy space charges of opposite signs are formed at the crests and troughs as shown in the figure. While the torques due to dielectric anisotropy and elasticity tend do stabilise $\vec{n}$, the transverse electric field due to the space charges tends fa distort it. At the same time the external field acts on the space charges and beyond a certain threshold voltage material flow sets in the sample. On the basis of this model and assuming the variation of deformation only in one direction (X), Helfrich derived an expression for the threshold voltage for the formation sf domains

$$V_{th} = 2\pi\left[\frac{k_{33}\,\pi}{\left(\frac{K_1\varepsilon_{\parallel}}{\eta_1}\right)\left(\frac{\varepsilon_{\perp}}{\varepsilon_{\parallel}} - \frac{\sigma_{\perp}}{\sigma_{\parallel}}\right) + (\varepsilon_{\parallel} - \varepsilon_{\perp})\left(\frac{\sigma_{\perp}}{\sigma_{\parallel}}\right)}\right]^{\frac{1}{2}} \qquad (8.1)$$

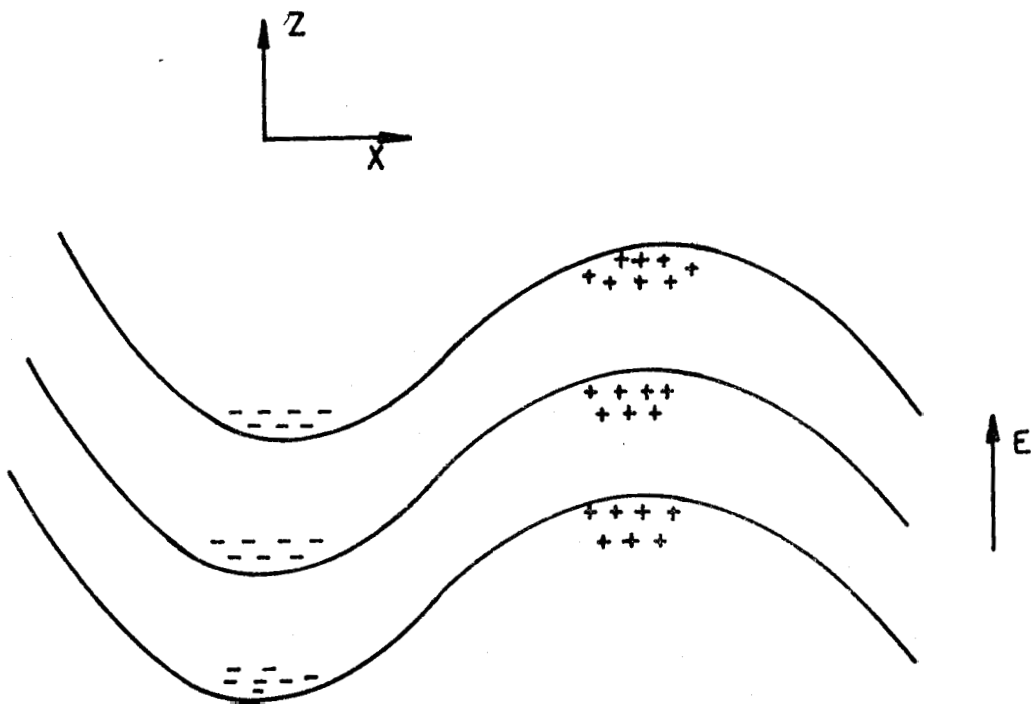

Figure 8.2

Bend fluctuations in a nematic giving rise *to* the segregation of opposite charges in the presence of electric field, eventually resulting in the electrohydrodynamic instability.

where k_{33} is the bend elastic constant, $\varepsilon_{\parallel}$ and $\varepsilon_{\perp}$, and $\sigma_{\parallel}$ and $\sigma_{\perp}$ the dielectric constant and electrical conductivity along and perpendicular to $\vec{n}$. X_1 and η_1 are viscosity coefficients.

The theory was extended to A.C. fields by including time dependent solutions (Dubois-Violette et al. 1971). At D.C. and low frequency A.C., the space charges are able to follow the field. As the frequency of the electric field is increased charge relaxation takes place at a certain frequency ω_T called the cut off frequency. ω_T is found to increase linearly with sample conductivity (Orsay Liquid Crystals Group 1971). As the frequency approaches ω_T, the threshold voltage for domain formation increases sharply. Above ω_T another type of pattern is observed beyond a field threshold. These optical patterns are called 'chevrons'. This region corresponds to tho 'fast turn off mode' (Heilmeier & Helfrich 1970).

Pens and Ford (1972) made computer calculations to explain D.C. and low frequency instability, taking ink, account the deformation varying along undistorted $\vec{n}$ as well as along the applied field direction. The resulting vortices are shown in figure 8.3 along with

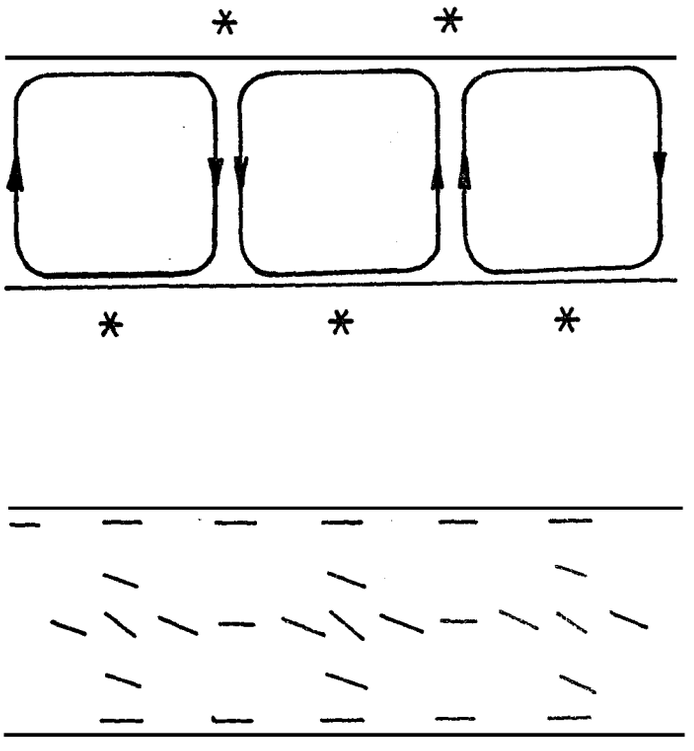

Figure 8.3

Cross-sectional view of the electrohydrodynamic flow patterns in the sandwich *geometry*. The top figure shows the velocity vector while the lower one shows the molecular alignments. The stars show positions of bright lines in the field of view as seen from top or bottom.

the orientation patterns of $\vec{n}$. The motion in adjacent vortices are of opposite sense. Purely from geometric considerations, one can see that the domain width is comparable to the sample thickness (also the electrode separation).

Electrohydrodynamic instabilities can also occur in materials with positive dielectric anisotropy under certain conditions as have been observed by De Jeu et al. (1971), Gruler and Meier (1972) and Gruler (1974).

In another experiment Williams (1972) applied an electric field to a nematic with negative dielectric anisotropy by using two parallel strips of conducting coating. The molecules were initially aligned parallel to the strips and hence normal to the electric field. The observation was made normal to the sample plane. Beyond a voltage threshold striations normal to the undistorted $\vec{n}$ are seen. The domains were seen only in polarised light. In this geometry the sample thickness was small compared to the electrode separation. Moreover the threshold voltage was large ($\sim$ 2000 V).

A new pattern

We have found the electrohydrodynamic flow patterns in a different geometry in which the

undistorted director is perpendicular to the electric field, the direction of observation being along $\vec{n}$ and normal to $\vec{E}$. Observations using a similar geometry have been independently reported by Chang (1973).

Experimental

(i) Set up I : The schematic diagrams of the set up are shown in figure 8.4. Two strips of copper or plastinum foils were held between two rectangular blocks of teflon. In these blocks rectangular holes were cut so that two small glass plates could be placed on both sides of the metal foils. The strips of foils were adjusted to be parallel (to $\sim \pm$ 10 μm), so that they formed the electrodes. The whole assembly was enclosed between two copper blocks. To avoid problem arising due to temperature gradient the experiments were done using a room temperature nematic, MBBA. The figures 8.4a and 8.4b give the cross-sectional view of the experimental set up in two different planes.

Homeotropic alignment of the sample was achieved by treating the surfaces of the glass plates with lecithin. The sample was injected into the space

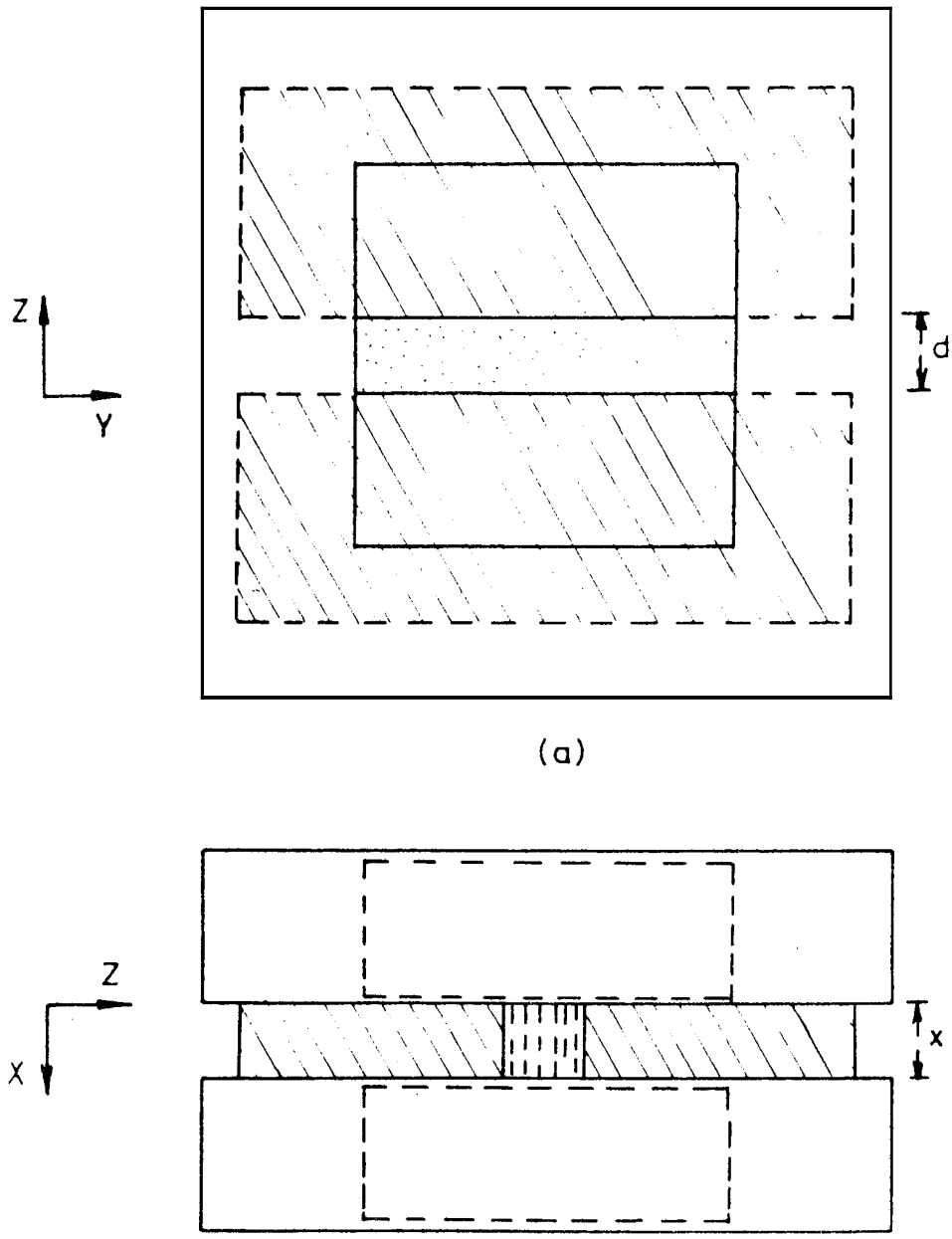

Figure 8.4: Sectional views of the set up used in *the* present study to observe the flow patterns. Direction of observation is along X axis. Field is applied along Z axis. The striped areas represent the metal foil electrodes. The sample is contained between plane glass plates. Electrode separation is d and sample thickness is x. Homeotropically aligned sample is indicated by dots in (a) and discontinuous lines in (b).

between the glass plates and the electrodes by means of a capillary tube.

As shown In the figure 8.4 the electric field is applied along Z. The undistorted director is along X. The observations are made through a polarizing microscope in the same direction. The field in this case is not strictly homogeneous because of the fringe effects. However since the compound used for tho experiment was conducting, this effect should be small. Nevertheless, to avoid any uncertainty in the interpretation of the observation it was felt worthwhile to repeat the observations in a truly uniform field and to compare them with the above results. For this reason another set up was used.

(ii) Set up II : The schematic diagrams are shown in figure 8.5. Two rectangular pieces (2 mm x 8 mm) of a microscope cover slip whose edges were polished, were pasted onto two wider (5 mm) conducting glass plates. They could be assembled with an open gap of rectangular arose section (figure 8.5). The assembly was placed in a rectangular groove cut in a copper block. The distance between the coverslips could be adjusted by simply shifting one of the glass plates parallel to, its breadth. This distance forms the

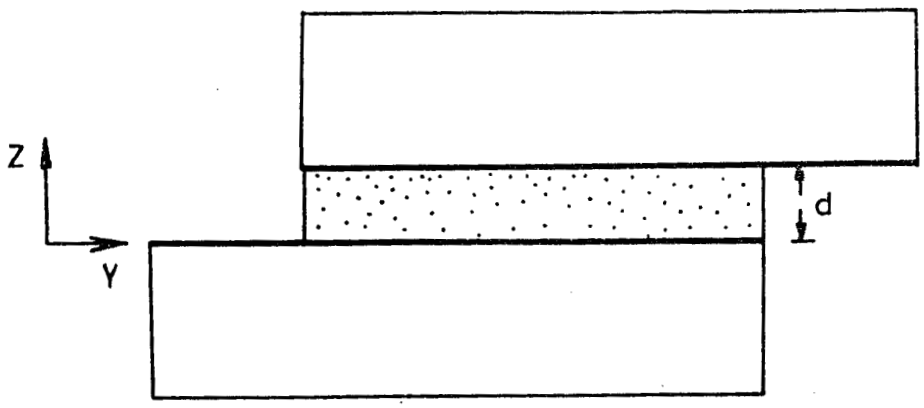

(a)

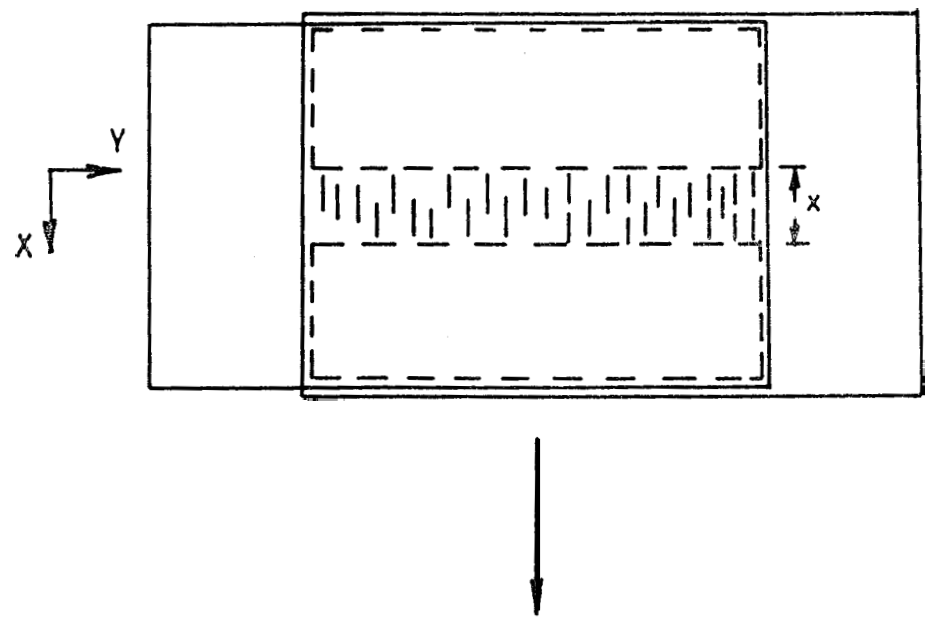

(b)

Figure 8.5: Sectional views of tho set up to observe electrohydrodynamic patterns using uniform electric fiold applied along the Z axis. The electrode separation is d and sample thickness is x. Arrow shows the direction of observation (X axis).

thickness of the sample (x). The cover slip thickness decides the distance between the electrodes (d). Figures 8.5a and 8.5b show the cross sections in different planes.

Relatively impure MBBA which had a resistivity $\sim 10^9$ ohm cm was used in these experiments.

Observations

We shall first present the observations made in set up I. Both copper and platinum electrodes were used in these studies. When observed between crossed polarizers, in the absence of any applied field, the field of view is dark. We shall now describe in detail the observations made with 30 μm thick copper electrodes separated by a distance of 150 μm. The electrohydrodynamic patterns are illustrated in figure 8.6.

When a D.C. field is applied, turbulence slowly sets in at $\sim$ 35 V. After some time ($\sim$ 10 minutes) these motions settle down to give a complicated periodic pattern (figures 8.6a and 8.6b).

For 20 Hz A.C., as the voltage is increased, the field of view begins to brighten up at $\sim$ 24 V.

Figure 8.6

Electrohydrodynamic patterns in MBBA. The set up is as in figurer 8.4. The electric field applied *between* copper electrodes is vertical and the director in the undistorted sample is along the direction of observation. The arrows on the right hand side indicate the settings of the nicols. x 30 μm, d 150 μm. *(a)* and (b) D.C. 35 V; (c), (d) and (e) *20* Hz, 32V; (f) and (g) 100 Hz, 45V.

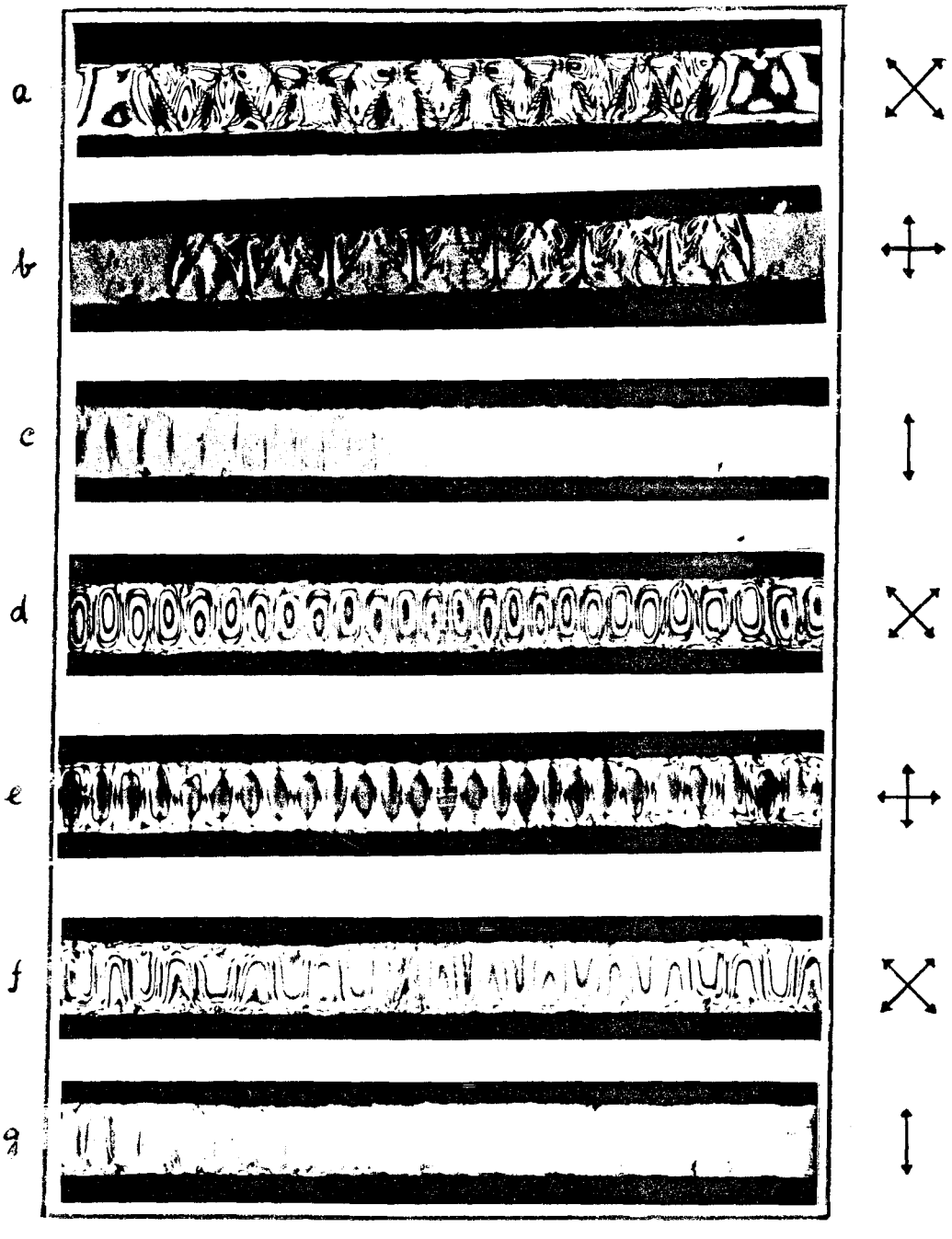
a
b
c
d
e
f
g

As the voltage reaches 28 V domains start forming. These domains are not very distinct and do not have a regular periodicity. At 30 V the domains are clearly seen and the bigger domains split up into small ones. The domain width is nearly uniform and approximately half the distance between the electrodes. In the absence of the analyser A and with the polarizer P set parallel to $\vec{E}$, equidistant lines parallel to $\vec{E}$ are seen (figure 8.6c). Figures 8.6d and 8.6e show the cellular patterns for different settings of the P and A.

Now Sf tho frequency of the applied field is increased to 100 Hz, tho threshold voltage V_c at which the domains start forming increases. When a regular pattern is obtained it lo wavy in nature (figure 8.6f). When viewed in the absence of the analyser and with polarizer axis set parallel Lo $\vec{E}$ the pattern looks as shown in figure 8.6g. As the frequency Po increased still further, the amplitude of the wavy pattern decreases and for high frequencies ($\sim$ 2 KHz) no pattern is seen.

For D.C. and low frequency A.C., as the voltage is increased, turbulence starts slowly and with further increase in voltage, dynamic scattering sets in.

The experiments with 40 μm thick platinum electrodes 200 μm apart give similar sequence of patterns as described above for a frequency *sf* 50 Hz.

In order to study the motion inside the patterns we chose a bigger set up with 100 μm thick platinum electrodes ~ 500 μm apart. At 50 Hz V_c is ~ 27 V (figure 8.7b). If there are tiny dust particles present in the sample one can see them moving in opposite directions parallel to $\vec{E}$ in adjacent domains. When the dust particles reach the electrodes they drift irregularly normal *to* $\vec{E}$ *to* the next domain and then move parallel to $\vec{E}$ towards the other electrode. Now 11 a dust particle moves along $\vec{E}$ very near one of the boundaries between two domains, it sometimes goes over to the adjacent domain, midway between its path and starts moving in tho opposite direction.

When the cross section of the incident beam is large, even if the polarizer is kept parallel to $\vec{E}$ and the analyser A is removed, the: field of view looks uniformly bright. However if the incident beam width is cut down, dark and bright equidistant patches show up. Now if P is kept normal to $\vec{E}$ the contrast la

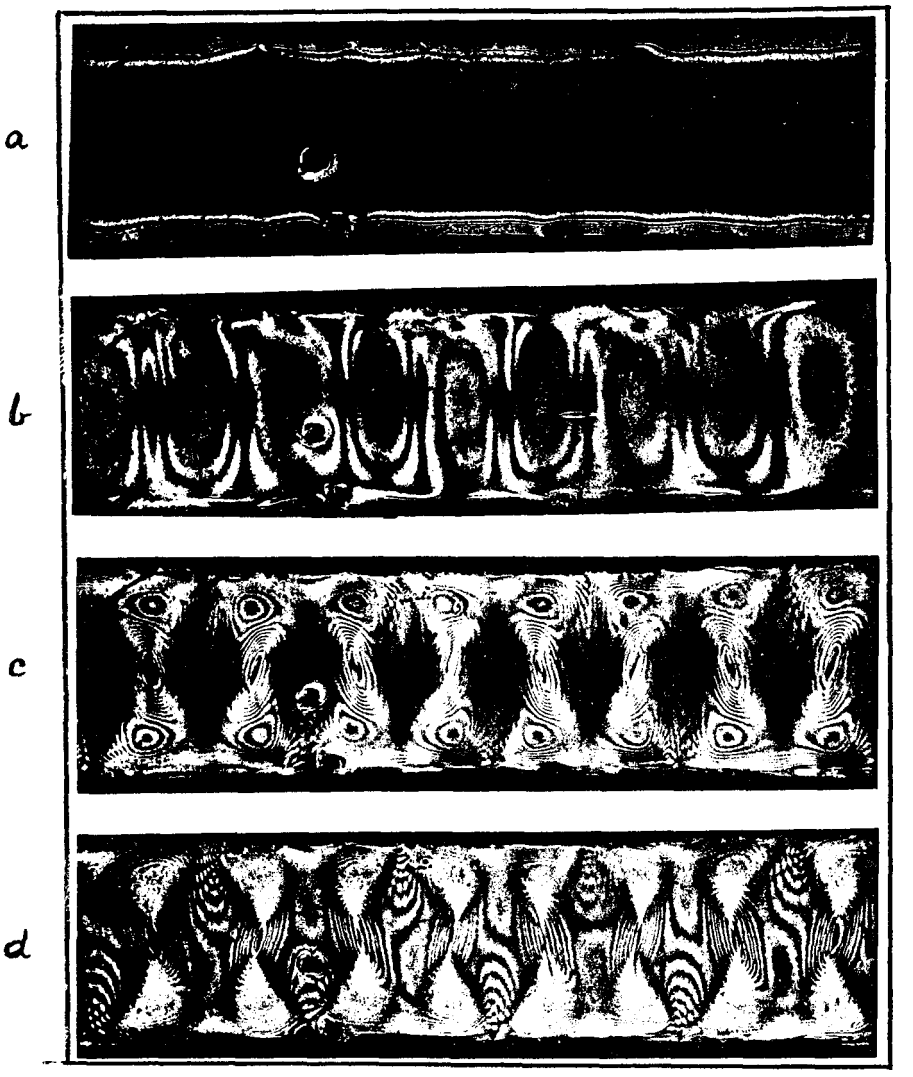

Figure 8.7

Electrohydrodynamic patterns in MBBA. Set up as in figure 8.4 with plantinum electrodes. x 100 μm, d 500 μm. Nicol settings are shown on right hand side. (a) 0 V, (b) 50 Hz 27 V, (c) and (d) 50 Hz, 33 V.

reduced although the patches could still be seen.

As the voltage is increased to 33V complicated patterns *ore* seen (figures 8.7c and 8.7d). The sharp boundary between two cellular domains seen at low voltages now transforms into a number of coaxial ellipses (figure 8.7c) in the central region between the electrodes. The dust particles moving midway between two sets of ellipses continue to move almost parallel to $\vec{E}$ as before. However if it comes near the elliptic pattern, it moves along one of the ellipses. Movement of dust particles in alternate sets of elliptic patterns show that they involve motions in opposite senses.

Now with P parallel to $\vec{E}$ and A removed, bright regular streaks (similar to figure 8.6c) are seen. These streaks are visible for any setting of P and A both crossed and parallel and even in the absence of P and A.

In all the set ups considered above, thin foils of metal are used as electrodes. Hence in XZ plane the field is not uniform because of fringe effects. In order to ascertain whether the above patterns are due to this effect or not we have repeated the experiments using uniform fields (figure 8.5).

We have made observations on two different sample thicknesses and electrode separations ($\sim$40 μm sample thickness (x) with electrode separation (d) $\sim$ 200 μm, and x $\sim$ 100 μm, d $\sim$ 750 μm). As the electric field is increased cellular domains are seen when 35 Volts (50 Hz) are applied between the electrodes. However, in this case V_c is slightly higher.

Discussion

A possible interpretation of the observed pattern is given below. In the usual sandwich geometry, the distance between the electrodes is a small fraction of the length available perpendicular to the field (X direction) and it is well known that *the* repeat distance in the cellular flow pattern is determined by the distance between the electrodes. Therefore several cells are formed with a periodicity along X axis. (Here undistorted $\vec{n}$ is along X and field is along Z (figure 8.1).) with vortices in neighbouring domains having opposite sense. However in the present configuration the distance between the electrodes is $\sim$ 5 times the space available in the lateral direction (X). Hence *it* is not possible to have more than one cell to be formed at any given value of the Y coordinate. It appears that in such

a case the neighbouring domains along Y direction assume opposite senses of rotation for low values of the applied voltage. In other words, under these conditions whereas in the usual geometry neighbouring domains with opposite senses of the vortices meet as shown in figure 8.8a, due to physical restrictions imposed by the present configuration they meet as shown in figure 8.8b.

Immediately above V_c, one sees domains of large widths. As mentioned earlier, as the field is increased bigger domains split up into smaller ones. It was observed that always a single domain splits up to form three domains. As the field is increased the cellular domains give way to complicated patterns. The movement af the dust particles shows that in addition to the opposite vortices mentioned above, there is also motion fa the plane YZ, whose sense is also opposite in alternate domains.

Recently Kai et al. (1975) observed that in the usual sandwich geometry, a new type of pattern called 'the grid pattern' can be seen sometime after the application of the field. They attributed this to a a three dimensional flow patterns. Our observations also confirm such a conclusion.

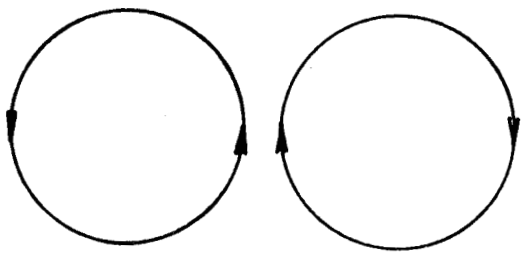

(a)

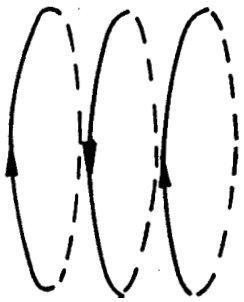

(b)

Figure 8.8

(a) Tho vortices in the sandwich geometry.
(b) Suggested disposition of *the* vortex patterns in the new geometry.

We shall summarise some of the features of the, patterns seen hers as compared to the ones observed by other workers. In the first place, we observe that the threshold voltage (~ 25 V) is much greater than that in the sandwich geometry. This could be due to the larger separation between the electrodes. We might mention here that Williams (1972) observed a 2000 V threshold when the electrode separation was $\sim$ 1 mm. The patterns observed here can be seen for any setting of the polarizers - parallel or crossed - and even in the absence of the polarizer and analyser. Moreover the D.C. field gives rise to complicated patterns. This could be *duo* to the charge injection.*

We now describe another interesting observation made on nematic droplets of MBBA under the influence of electric fields.

Distortions of nematic droplets

If *the* temperature of the sample (relatively impure MBBA) is maintained at the nematic-isotropic transition point (T_{NI}), nematic droplets can be seen suspended in *tho* isotropic phase. In the absence *of* any external field they look circular in cross section (figures 8.9a). (In the actual situation, since *the*

*After this work was completed, we came across a report by Cheng (1973) where essentially similar observations have been described.

Figure 8.9

Electrohydrodynamic distortions of nematic droplets of MBBA suspended in the isotropic phase a+, the transition temperature. (a) undistorted droplets under zero field; (b) 100 Hz, 80 V; (c) 100 Hz, 100 V; (d) 100 Hz, 250 V; (e) 500 Hz, 100 V; and (f) 1 KHz, 100 V.

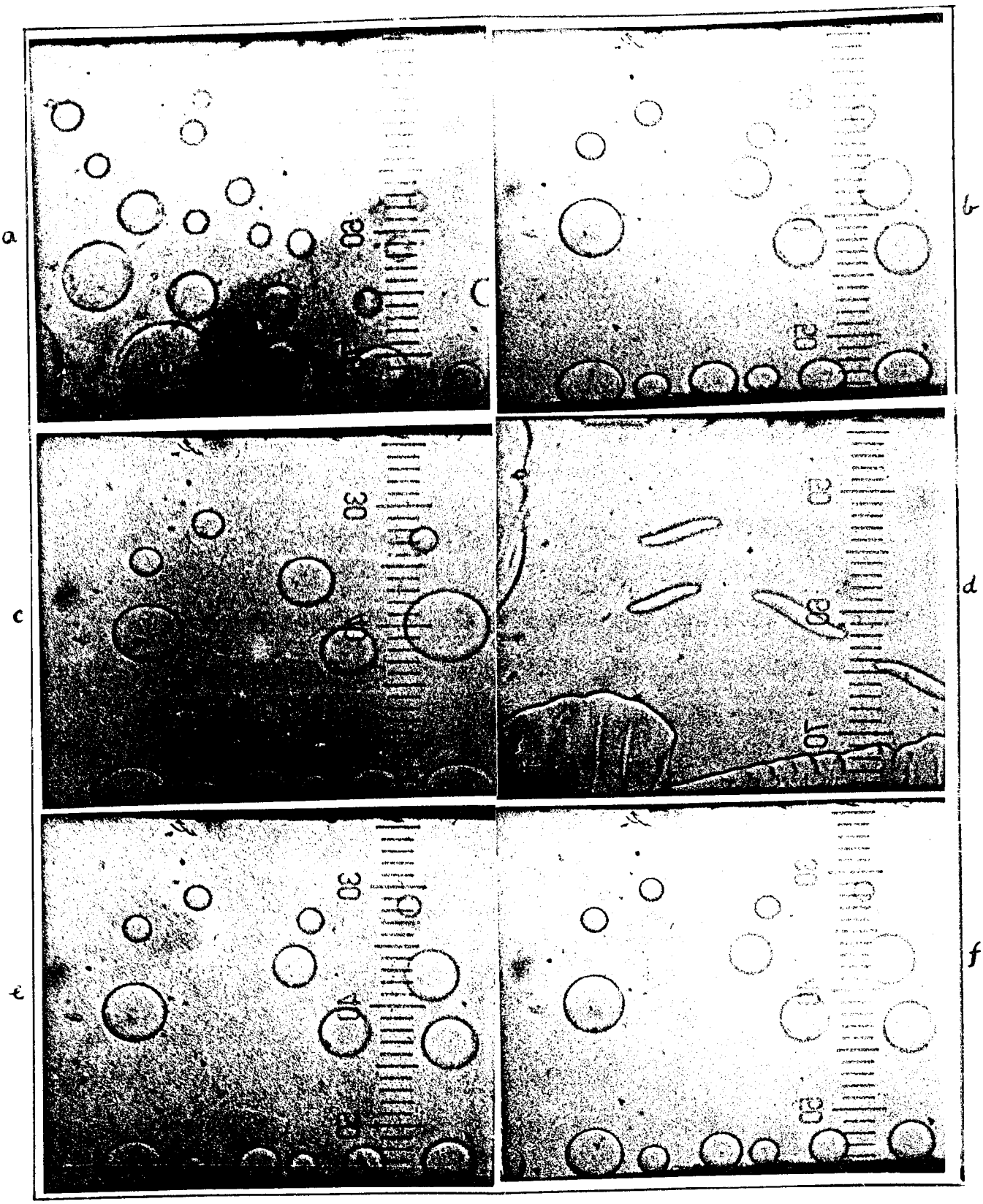
a
b
c
d
e
f

sample thickness is small, the droplets are discs of nematic in the isotropic medium.)

The same experimental set up as described earlier in this Chapter was used. The effects of uniform field (set up II) as well as the non-uniform field (set up I) are similar.

If a D.C. or a low frequency A.C. electric field is applied, the droplets get deformed to elliptic shapes as the voltage exceeds a threshold value (figure 8.9b). However this threshold could not be detected since the deformation of the droplets woe gradual. The major axis of the ellipse was always found to be perpendicular to the electric field direction. With the increase in the voltage, the ellipticity increase (figure 8.9c). However it was found that for any voltage, the ellipticities of different drops were not uniform. In addition to the deformations the droplets themselves move along $\vec{E}$ from one electrode to another. If two tiny droplets are found to move la opposite directions and appear La move along one line parallel to $\vec{E}$, they move poet each other without touching each other. This indicates that there is a vortex motion in the XZ plane. As the voltage is increased, the velocities of the drops also increase.

If a dust particle is present in one of the droplets, it is found to move inside the droplet in vortices. Hence it appears that there are two kinds of vortices - one confined to the XZ plane in the isotropic bulk, which causes the movement of the drops, and another vortex inside each nematic droplet.

As the voltage is increased considerably, the drops take peculiar, quickly changing shapes (figure 8.9d). Now the droplets move in all sorts of directions. Movement of dust particles in the isotropic bulk is haphazard.

With increasing frequency, the voltage necessary to deform the droplets increases (figure 8.9e) and for very high frequencies, no deformation can be observed even at high voltage (figure 8.9f).

The existing theory (Felici 1969) for the electric field induced instabilities in isotropic liquid based on the charge injection phenomena cannot be applied here because, the vortex motion is observed even for A.C. ($\sim$ 100 Hz). It is clear that the origin of the deformation is electrohydrodynamic, but we have not attempted to give any explanation for the phenomena.

References

Carr, E.F. 1963 J. Chem. Phys. 39, 1979.

Chang, R. 1973 Mol. Cryst. Liq. Cryst. 20, 267.

De Jeu, W.H., Gerritsma, C.J. and Van Doxtel, A.M. 1971 Phys. Lett. 34A, 203.

Dubois-Violette, E., de Gennes, P.G. and Parodi, O. 1971 J. de Phys. 32, 305.

Felici, N. 1969 Rev. Generale d'Elect. 78, 717.

Freedericksz, V. and Zolina, V. 1933 Trans. Faraday Soc. 29, 919.

Greubel, W. and Wolff, U. 1971 Appl. Phys. Lett. 19, 213.

Gruler, H. and Meier, G. 1972 Mol.Cryst.Liq.Cryst. 16, 299.

Gruler, H. 1974 Mol. Cryst. Liq. Cryst. 27, 31.

Heilmeier, G.H., Zanoni, L.A. and Barton, L.A. 1968 Proc. IEEE 56, 1162.

Heilmeier, G.H. and Helfrich, W. 1970 Appl. Phys. Lett. 16, 1955.

Helfrich, W. 1969 J. Chem. Phys. 51, 2755.

Helfrich, W. 1969 J. Chem. Phys. 51, 4092.

Kai, S., Yamaguchi, K., Hirakawa, K. 1975 Japan J. Appl. Phys. 14, 1385.

Kai, S., Yamaguchi, K. and Hirakawa, K. 1975 Japan J. Appl. Phys. 14, 1653.

Kast, W. 1931 Z. Physik 71, 39.

Orsay Liquid Crystal Group 1971 Mol.Cryst.Liq.Cryst. 12, 251.

Penz, P.A. and Ford, G.W. 1972 Phys. Rev. A6, 414.

Smith, I.W., Galerne, Y., Lagerwall, S.T., Dubois-Violette, E. and Durand, G. 1975 J. de Phys. 36, C1-237.

Williams, R. 1963 J. Chem. Phys. 39, 384.

Williams, R. 1972 J. Chem. Phys. 56, 147.

Zwetkoff, V.N. and Mikhailov, G.M. 1938 Acta Physicochim. URSS 8, 77.

APPENDIX I

POINCARE SPHERE

We summarize those features of the Poincare sphere representation (see Ramachandran and Ramaseshan 1961) which have been made we of in Chapters I and If.

Any general state of polarization of a light beam can be defined by two quantities: (i) *the* orientation of the major axis of the ellipse called the azimuth and is specified by its angle λ with any direction in the wavefront, (ii) the ratio of the axes of the ellipse $\frac{b}{a}$ ($b < a$). The ellipticity ω is given by the equation $\tan \omega = \frac{b}{a}$.

The states of polarization can be represented by a point on the surface of a sphere of unit radius, whose latitude and longitude have values 2ω and 2λ. Such a sphere is called Poincare sphere (figure 1) (Poincare 1892).

In the figure H and V represent horizontal and vertical linearly polarized light. In general, all linear states sf polarization are represented by points on the equator HCVD, the longitude being equal to twice the angle made with the horizontal direction. Therefore the points C and D correspond to linear

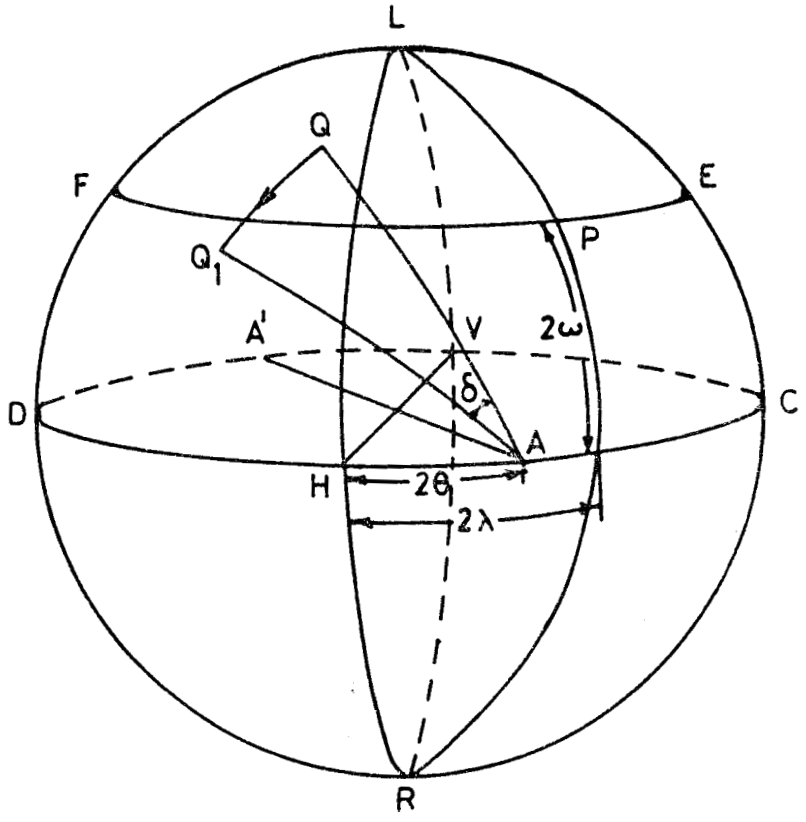

Figure 1

The Poincare sphere showing the states of polarization of a light beam after it traverses a phase retarder.

vibration at $\pm \frac{\pi}{4}$. L and R are the poles of the sphere and represent left and right circular vibrations respectively. All elliptic states having the same orientation (λ) of their major axes are represented By points on the meridian LPR of longitude 2λ. Also all the elliptic states with the same ellipticity (ω) are represented by points om the latitude circle EPF of latitude 2ω.

Passage of light through a birefringent medium

Let A and A' represent the fast and slow axes of the birefringent plate respectively. A makes an angle Θ with the horizontal and hence HA is 2Θ. Let Q be the polarisation of the light incident on the plate. δ is the phase difference between extraordinary and ordinary vibrations when light traverses the plate. On the Poincare sphere the polarisation of the emergent light is represented by the point Q_1, obtained by rotating the point Q about the line AA' through an angle δ in the anticlockwise direction. However if A is the slow axis, the rotation is in the clockwise direction.

References

Poincare, H. 1892 Theorie Mathematique de la Lumiere, Vol. II, Chap. XII

Ramachandran, G.N. and Ramaseshan, S. 1961 'Crystal Optics', Handbuch der Physik, Vol.XXV/1, Ed.S.Fluge (Springer-Verlag).

APPENDIX II

DETERMINATION OF THE REFRACTIVE INDICES AND ORIENTATIONAL ORDER PARAMETERS OF NEMATIC LIQUID CRYSTALS

In this appendix we give the experimental details of measuring the refractive indices of nematic liquid crystals and the method of estimating the orientational order parameter and density using the measured data.

Orientational order parameter

A nematic liquid crystal has long range orientational order which is intermediate between that of a perfectly ordered crystal (S=1) and of a disordered liquid (isotropic liquid: S=0). If θ is the angle made by any molecule *pith* the director $\vec{n}$, then the order parameter of the medium l a given by (Zwetkoff 1942)

$$S = \frac{\overline{3\cos^2\theta - 1}}{2} \qquad (1)$$

The bar denotes a statistical average. Let $\alpha_{\parallel}$ and $\alpha_{\perp}$ be the polarizabilities parallel and perpendicular to the long axis of the molecule. Then the polarizabilities of the medium as a whole, along and perpendicular to

the director are respectively given by

$$\alpha_e = \bar{\alpha} + \frac{2}{3}(\alpha_{\parallel} - \alpha_{\perp})S$$

$$\alpha_o = \bar{\alpha} - \frac{1}{3}(\alpha_{\parallel} - \alpha_{\perp})S \qquad (2)$$

Hence

$$S = \frac{\alpha_e - \alpha_o}{\alpha_{\parallel} - \alpha_{\perp}} \qquad (3)$$

There have been two different approaches to relate α_e and α_o with n_e and n_o, viz., Neugebauer's formula (1950) and Vuks formula (1966). The values of S calculated using these two methods agree very well (see for example, Subramanyam and Krishnamurti 1973). Vuks formula is simpler of the two. Moreover we should have an independent measurement of the temperature variation of the density to be able to use Neugebauer's relation, while It turns out that Vuks formula itself can be used to derive this data from the optical measurements. Hence we have wed Vuks formula in all our calculations.

Vuks formula

Vuks found that the Lorenz-Lorentz formula works well for the average polarizability of strongly anisotropic organic (molecular) crystals

$$\frac{\overline{n^2} - 1}{\overline{n^2} + 2} = \frac{4\pi}{3}\gamma\,\bar{\alpha} \qquad (4)$$

where

$$\overline{n^2} = \frac{n_x^2 + n_y^2 + n_z^2}{3}$$

$$\bar{\alpha} = \frac{\alpha_x + \alpha_y + \alpha_z}{3}$$

n_x, n_z and α_x, α_y, α_z being the principal refractive indices and polarizabilities respectively and γ a the number of molecules/cc.

We can write equation (4) as

$$\frac{n_x^2 - 1}{\overline{n^2} + 2} + \frac{n_y^2 - 1}{\overline{n^2} + 2} + \frac{n_z^2 - 1}{\overline{n^2} + 2} = \frac{4\pi}{3}\gamma(\alpha_x + \alpha_y + \alpha_z) \qquad (5)$$

which is found to be experimentally valid in several cases.

In an isotropic medium the polarizability

$\vec{P} = \frac{n^2 - 1}{4\pi} \cdot \vec{E}$ where is the applied field.
Also if F is the internal field

$$\vec{P} = \alpha\gamma\vec{F} = \frac{\alpha\gamma(n^2 + 2)}{3}\vec{E}$$

For anisotropic materials

$$P_i = \frac{n_{ik}^2 - \delta_{ik}}{4\pi} E_k \qquad i,k = x,y,z.$$

Assuming that the internal field in the crystal is the same in all directions, we can write

$$P_i = \frac{\gamma}{3} (\overline{n^2} + 2)\, \alpha_{ik} E_k$$

From these two equations we get

$$\frac{n_i^2 - 1}{\overline{n^2} + 2} = \frac{4\pi}{3} \cdot \gamma\, \alpha_i \qquad (6)$$

This is the Vuks formula. One can see that this leads to the equation (5).

From equations(3) and (6)

$$S = \frac{\bar{\alpha}}{\Delta\alpha} \cdot \frac{n_e^2 - n_o^2}{\overline{n^2} - 1} \qquad (7)$$

where $\Delta\alpha = \alpha_{\parallel} - \alpha_{\perp}$.

From equation (4)

$$\frac{\overline{n^2} - 1}{\overline{n^2} + 2} = \frac{4\pi}{3} \cdot \frac{N\rho}{M} \cdot \bar{\alpha}$$

where N is the Avagodro number, ρ is the density and M is the molecular weight. Hence the density

$$\rho = \frac{3}{4\pi} \cdot \frac{M}{N} \cdot \frac{1}{\bar{\alpha}} \cdot \frac{\overline{n^2} - 1}{\overline{n^2} + 2} \qquad (8)$$

We shall now describe the experimental set up to measure *the* refractive indices of nematic liquid crystals.

Experimental

We have used the prism method (Pellet and Chatelain 1950, see also Madhusudana, Shashidhar and Chandrasekhar 1971) by which n_o and n_e can be measured in a single setting.

Construction of the prism

A small angled glass prism is obtained by placing two rectangular glass plates one *over* the other, with a thin strip sf glass placed In between them at one end and parallel to the width of the plates (figure 1). The sandwiched strip is cemented to the glass plates by Araldite (Cibatul (India) Ltd.). It is important to note that the strip is *of* uniform thickness along its length. This ensures that when a light beam is incident on Plate I of the prism (figure 1) normal to its refracting edge, the rays reflected by both the plates and the incident ray all lie in the same plane. In order *to* avoid any contamination of liquid crystals by araldite, care is taken to see that it does not come into contact with the sample.

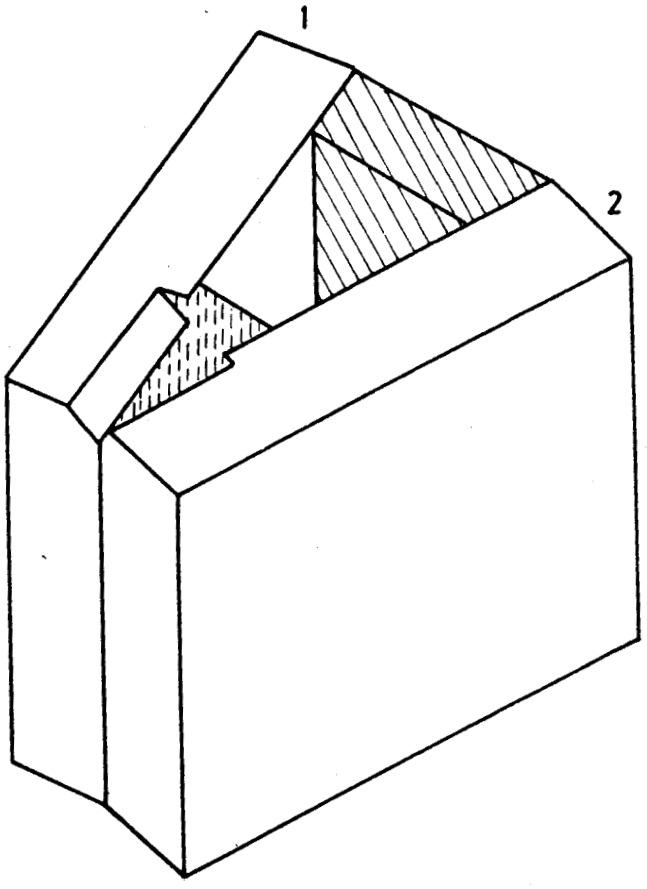

Figure 1

Small angle prism made of two optically flat glass plates 1 and 2 cemented together with a strip of glass (shorn by a striped region) used as spacer at one end. The glass flats are bevelled near the refracting edge of the prism *to* facilitate filling of the liquid, indicated by the region shaded by dashed lines.

The glass plates used for the prism should have perfectly parallel surfaces, in addition to being optically flat. For the proper choice of the glass plates a goniometer spectrometer provided with a gaussian eye-piece is used. The eye-piece is provided with a source of light, the light beam from which moves away from the eye-lens along the axis of the telescope. A glass plate head in front of the telescope objective reflects this light and an illuminated cross is seen in the field of view of the eye-piece. If the glass plats does no2 have parallel surfaces, two crosses reflected by the two surfaces are seen. Moreover *if* the surfaces are not optically flat, the images are blurred. Hence only those glass plates are chosen which when held in front of the telescope give a single, clear reflected cross.

The angle of the prism used is $\sim$ 5° and its dimensions are $\sim$ 10 mm x 7 mm.

Oven and sample holder

The prism is enclosed in a chamber so as to be in good thermal contact with blocks of copper (figure 2a). However, in order to avoid any contamination of the sample due to the contact with copper,

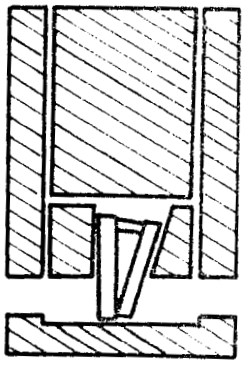

(a)

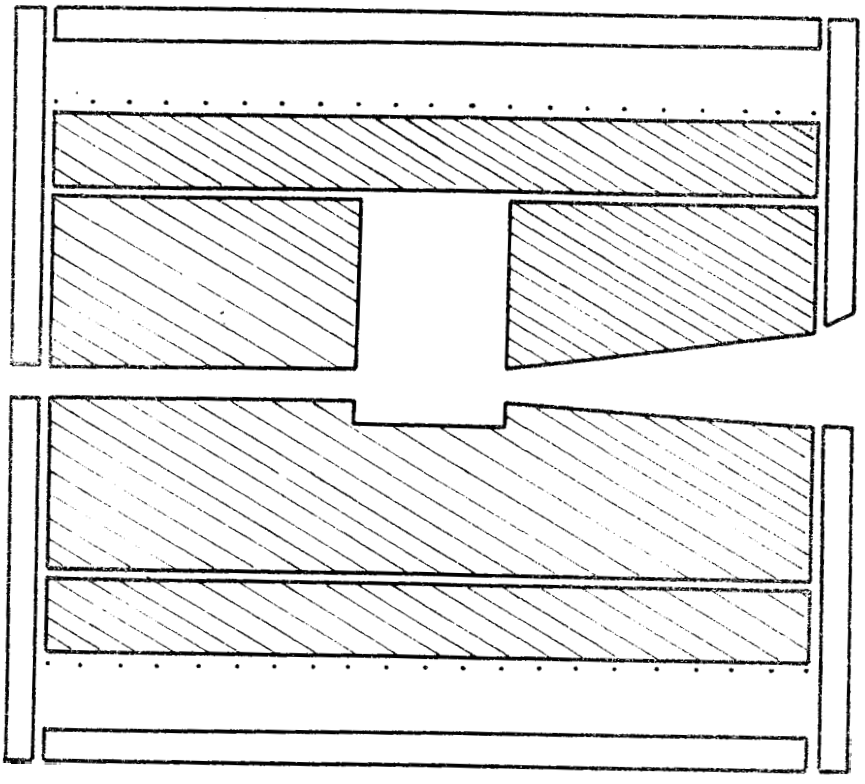

(b)

Figure 2

(a) Copper holder for the prism

(b) Heater with large blocks of copper surrounding the sample holder. Striped areas represent copper. The outer surface of the heater is thermally insulated.

thin sheets of teflon ($\sim$ 100 μm) are placed around the prism so that the sample does not come into direct contact with copper. The copper chamber in turn is placed inside a massive copper block of rectangular cross section, through which a hole (4 mm x 4 mm) is drilled to allow light to fall on the prism (figure 2b). The light after refracting through the sample emerges out of the block through a diverging aperture (figure 2b) to enable us to measure the angles of deviation. The whole block is placed inside an oven with 1 cm thick inner copper walls. The heater wire is wound uniformly and the oven is heated by lead accumulators so that a steady current can be drawn from them. On both ends of the heater, the copper block is covered by sheets of bakelite *to* avoid heat loss and minimise any temperature gradients along the length of the block.

Sample preparation

The rubbing technique Is used *to* get an oriented sample. The best results are obtained when a thin strip of polythene sheet is used to rub against the inner surfaces of the glass plates unidirectionally. parallel *do* the refracting edge. In addition, the sample 3s introduced into the prism in the nematic

state by means of a capillary and is allowed to flow in the direction of rubbing. Typically the sample occupies a width of ~ 2-3 mm from the refracting edge (figure 1). The test for good orientation is done by observing the sample between two crossed polarizers through a low powered microscope. Since only a part of the aperture is filled with the sample, both direct light as well as the light refracted by the sample can be received by the telescope while measuring the refractive indices.

Temperature measurement and control

The temperature is measured as described in Chapter II. The bat junction sf the thermocouple is kept in contact with the prism. The cold junction is kept in melting ice formed from distilled water.

Sufficient time is allowed to elapse between two sets of readings for different temperatures so that the temperature change is within ±0.1°C over ~ 45 minutes which is the time taken for one complete set of readings. (We have made measurements for 3 wavelengths. For each wavelength 4 sets of readings are taken. Each set consists of 4 readings. The scatter in readings is ± 3 sec of arc.)

Measurement of refractive indices

The refractive indices were measured by means of a precision goniometer spectrometer (PRAZISIONS MECHANIK, East Germany) reading to 2" of arc.

Before making any measurements the position of the prism is adjusted so that its refracting edge is vertical (i.e., parallel to the slit) with the help of the gaussian eyepiece. The light reflected by plates 1 and 2 of the prism (figure 3a) form images of illuminated crosses. The levelling screws 04 the prism table are properly adjusted until the points of intersection of the crosses lie in one horizontal plane. When this is done the angle between the crosses is equal to the angle A of the prism.

The refractive indices were measured by the normal incidence method, i.e., the plate 1 of the prism is set normal to the incident beam (figure 3b). Now the incident wave on entering the sample, splits into the ordinary and extraordinary vibrations, travelling at different velocities, forming two distinct images in the focal plane of the eyepiece. For a well oriented sample, these images are sharp. To reduce any spread of the image due to temperature gradient in the sample, the vertical width of the

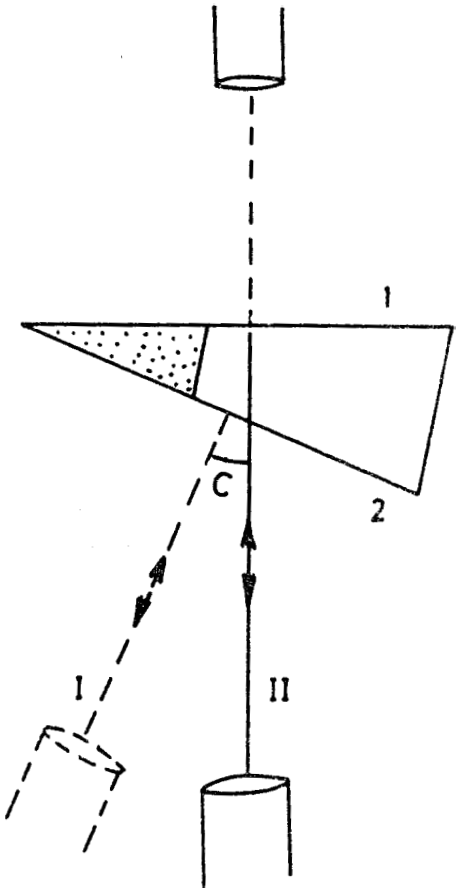

Figure 3a

Schematic diagram of the setting of the prism so that plate 1 is normal *to* the incident light. Figure indicates the path of the light beams reflected by plates 1 and 2.

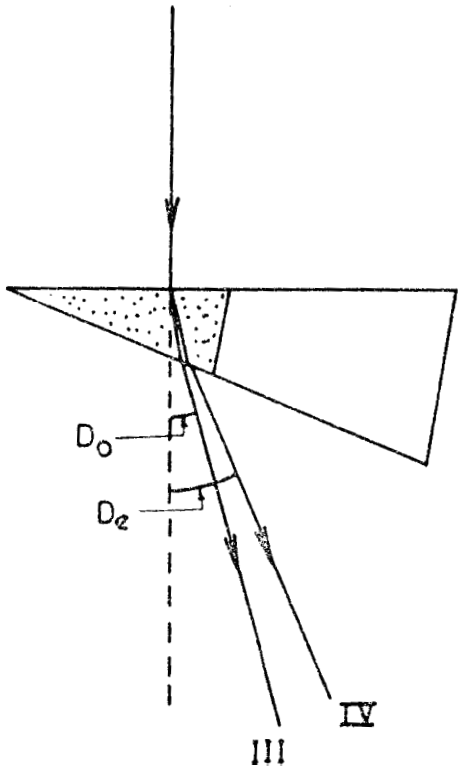

Figure 3b

Refraction of the ordinary and extraordinary rays through the prism. D_o and D_e are the respective angles of deviation.

incident beam was reduced to $\sim$ 2 mm. Whenever a set of measurements were taken the check for normal incidence was done. Each time the angle of the prism was measured. The readings were taken in the order I, II (figure 3a), III and IV (figure 3b) so that the error due to backlash was avoided*

If A is the angle of the prism, n_o and D_o, and n_e and D_e are the refractive index and angle of deviation for ordinary and extraordinary vibrations respectively for a wavelength λ, then

$$n_o = \frac{\sin(A + D_o)}{\sin A}$$

$$n_e = \frac{\sin(A + D_e)}{\sin A} \qquad (9)$$

We have measured the refractive indices for three different wavelengths, namely, λ 5461 Å, λ 5893 Å and λ 6328 Å.

The data on refractive indices are given in the relevant chapters.

Measurement of density

In the case of 5CB and 7CB we used a small specific gravity bottle ($\sim$ 6.5 cc in capacity) to

weigh the sample. The sample was weighed using the semimicrobalance SAEM68 (Labor Küstner, East Germany), the sensitivity of which is 10 micrograms.

In the case of 6OB, we could not adopt the above procedure for lack of sufficient quantity of the material. Hence a small length of (~ 1 cm) the sample was taken in a capillary tube and its length and mass were determined. The calibration in all cases was done against double distilled water. All the measurements were made at room temperature (25°C). The accuracy in specific gravity bottle method is ~ ±0.1% and that In capillary method ~ ±0.5%.

In the case of a compound which shows nematic phase at temperatures above the ambient, a small oven is used. A nichrome wire is evenly wound on a thick walled copper tube. The windings are surrounded by asbestos. It is enclosed in an aluminium tube which is mounted on a base provided with levelling screws. The temperature is maintained by passing a steady current for a long time using lead accumulators.

A slot ~ 2 mm in width is cut along the length of the tube to enable us to make measurements on the sample contained in a capillary tube. The length of

the sample pellet was measured using a travelling microscope. The calibration was done against PAA for which accurate density data are available.

We have measured the density of 8 OCB, 2 OMCPC and 8 OMCPC using this set up. The accuracy is only about $\sim 0.5\%$. The temperature is accurate to $\sim 0.5°C$. The density was measured at one temperature and the temperature variation of ρ was derived using the optical data (equation (8)).

The density data and the calculations are given in relevant chapters.

Order parameter

From equation (7) it is evident that for the absolute values S, we have to know $\bar{\alpha}/\Delta\alpha$. Using equation (8), $\bar{\alpha}$ can be obtained. If the value of S for any compound is known independently, $\bar{\alpha}/\Delta\alpha$ and hence $\Delta\alpha$ can be calculated. In order to calculate $\Delta\alpha$ for other compounds of the homologous series we adopt the following procedure.

In a homologous series of compounds with an alkyl end group, in the even members, the final C-C bond makes a large angle with the molecular axis

whereas in odd members the final C-C bond makes a small angle with the molecular axis. The change in $\Delta\alpha$ (i.e., $\delta(\Delta\alpha)$) in going from one to the next member of the series can be estimated from the knowledge of bond polarizabilities.

In estimating $\delta(\Delta\alpha)$ we assume for simplicity an all trans configuration of the chain (See Chapter III, figure . Further we assume that the last C-C bond in an odd member is along the molecular axis.

(a) Increment to $\Delta\alpha$ from an even to the next higher odd member

In going from even to odd member, one C-H bond is replaced by a C-C bond along the molecular axis and three C-H bonds equally inclined to the molecular axis are added. The configuration of the end group is shown in figure 4a.

Contributions from different bonds to the polarizability in units of 10^{-24} cm^3 are given below. The bond polarizabilities are taken from Hartshorne and Stuart (1970).

C-C bond: $\alpha_x = 0.97$, $\alpha_y = 0.25$, $\alpha_z = 0.25$. Therefore polarizability along X, $\alpha_{\parallel}$ * & = 0.97, @ polarizability perpendicular to X, $\alpha_{\perp} = \frac{\alpha_y + \alpha_z}{2} = 0.25$.

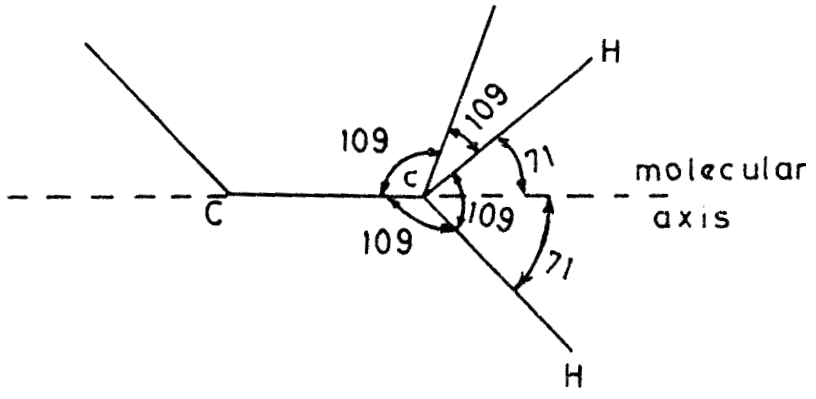

(a)

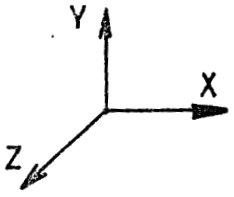

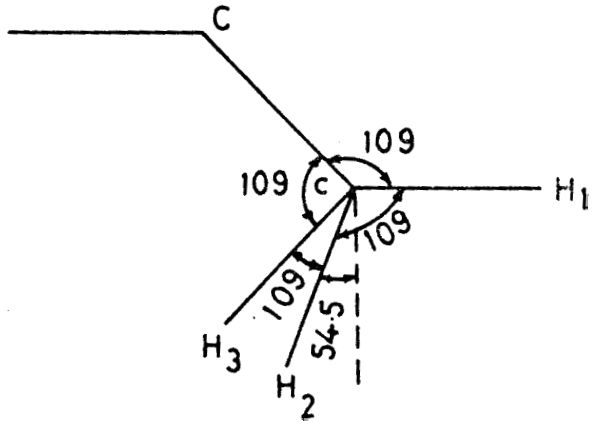

(b)

Figure 4

(a) Last segments of the end chain in the odd members of a homologous series having molecules with alkyl chains. An all-trans configuration is assumed with molecular axis along the final C-C bond.

(b) Last segments of the end chain in the even members of a homologous series having molecules with alkyl chains.

C-H bond (replaced by C-C bond).

$$\alpha_x = 0.82, \quad \alpha_y = 0.60, \quad \alpha_y = 0.60$$

$$\alpha_{\parallel} = 0.82, \quad \alpha_{\perp} = 0.60.$$

C-H bands equally inclined to X axis

$$\alpha_x = 0.82 \cos^2 71 + 0.60 \sin^2 71 = 2.62$$

$$a_y = 0.82 \sin^2 71 + 0.60 \cos^2 71 = 0.80$$

$$a, = 0.60$$

Therefore

$$\alpha_{\parallel} = 0.62, \quad \alpha_{\perp} = 0.70.$$

Therefore increment in polarizability along X,

$$\Delta\alpha_{\parallel} = 0.97 - 0.82 + 3(0.62) = 2.01$$

and increment in polarizability perpendicular to X,

$$\Delta\alpha_{\perp} = 0.25 - 0.60 + 3(0.70) = 1.75 .$$

Hence the increment in $\Delta\alpha$ on going from even to next higher odd member is

$$\delta(\Delta\alpha) = 0.26 .$$

(b) Increment to $\Delta\alpha$ between an odd and the next higher even member

The configuration of the end Group of an even member is shown in figure 4b.

C-C bond

$$\alpha_x = 0.97 \cos^2 71 + 0.25 \sin^2 71 = 0.33$$

$$\alpha_y = 0.97 \sin^2 71 + 0.25 \cos^2 71 = 0.89$$

$$\alpha_z = 0.25$$

Therefore

$$\alpha_{\parallel} = 0.33 , \quad \alpha_{\perp} = 0.57.$$

C-H bond (replaced by C-C bond)

$$\alpha_{\parallel} = 0.62 , \quad \alpha_{\perp} = 0.70$$

$C-H_1$ bond

$$\alpha_{\parallel} = 0.82 , \quad \alpha_{\perp} = 0.60$$

$C-H_2$ bond

$$\alpha_x = 0.82 \cos^2 54.5 \sin^2 35.5 + 0.60 \cos^2 35.5 + 0.60 \sin^2 54.5 \sin^2 35.5 = 0.63$$

$$\alpha_y = 0.82 \cos^2 54.5 \cos^2 35.5 + 0.60 \sin^2 35.5 + 0.60 \sin^2 54.5 \cos^2 35.5 = 0.65$$

$$\alpha_z = 0.82 \sin^2 54.5 + 0.60 \cos^2 54.5 = 0.75 .$$

Therefore

$$\alpha_{\parallel} = 0.63 , \quad \alpha_{\perp} = 0.70 .$$

Similarly for $C-H_3$ bond $\alpha_{\parallel} = 0.63$, $\alpha_{\perp} = 0.70$.

Hence the increment in polarizability along X axis

$$\Delta\alpha_{\parallel} = 0.33 - 0.62 + 0.82 + 2(0.63) = 1.79$$

and the increment in polarizability perpendicular to X axis

$$\Delta\alpha_{\perp} = 0.57 - 0.70 + 0.60 + 2(0.70) = 1.87.$$

Hence the increment in $\Delta\alpha$ on going from odd *to* next higher even member $\delta(\Delta a) = -0.08$.

Using these values of $\delta(\Delta\alpha)$, the Δa values for all members of the series can be calculated if $\Delta\alpha$ for any member is known independently.

The S values calculated using $\Delta\alpha$ derived from the above procedure are given in the relevant chapters.

Latent heat measurements

Latent heats of transitions were measured using a Perkin-Elmer DSC-2 (USA) differential scanning calorimeter. Since the compounds used were fairly low melting, cyclohexane was used as the standard. Typically, 5 mgs. of the sample were used in the measurements.

References

Hartshorne, N.H. and Stuart, A. 1970 'Crystals and Polarizing Microscope', p. 156 (Edward Arnold, London).

Madhusudana, N.V., Shashidhar, R. and Chandrasekhar, S. 1971 Mol. Cryst. Liquid Cryst. 13, 61.

Neugebauer, H.E.J. 1950 Canad. J. Phys. 18, 252.

Pellet, O. and Chatelain, P. 1956 Bull. Soc. Fr.Miner. Cryst. 73, 154.

Subramhanyam, H.S. and Krishnamurti, D. 1973 Mol.Cryst. Liquid Cryst. 22, 239.

Vuks, M.F. 1966 Optics and Spectroscopy 20, 361.

Zwetkoff, V. 1942 Acta Physicochim. URSS 16, 132.